# Patterns and factors of interannual variations of boreal summer intraseasonal oscillation intensity over tropical western North Pacific

Yuqi Wang[1,2] · Renguang Wu[1,3,4]

## Abstract

Present study analyzes spatial patterns and factors of interannual variations of 10–20-day and 30–60-day intraseasonal oscillation (ISO) intensity during boreal summer over tropical western North Pacific (WNP). The three leading modes of 10–20-day ISO intensity variation feature a southeast–northwest distribution, a southeast–northwest contrasting pattern, and large loading over the subtropics, respectively. The two leading modes of 30–60-day ISO intensity variation show a west–east distribution and a west–east dipole pattern, respectively. Three types of sea surface temperature (SST) influences are identified on the ISO intensity variation. One is a direct influence of El Niño–Southern Oscillation (ENSO) on seasonal mean background over tropical WNP via a Rossby wave type response. This type of influence is prominent on the leading mode of 10–20-day ISO intensity and the eastern portion of the second mode of both 10–20-day and 30–60-day ISO intensity. Second is an indirect influence of ENSO on seasonal mean background over subtropical WNP and the Maritime Continent through anomalous Walker circulation. This type of influence includes the western portion of the second mode of both 10–20-day and 30–60-day ISO intensity. Third is an influence of regional SST anomalies. Opposite SST anomalies in the North Indian Ocean and tropical North Pacific work together to modulate seasonal mean background over tropical WNP. This type of influence is prominent on the leading mode of 30–60-day ISO intensity. In addition, internal atmospheric process may play a role in 10–20-day ISO intensity change over subtropical WNP.

**Keywords** Intensity of intraseasonal oscillations · Interannual variation · Influence of SST anomalies · Impacts of internal atmospheric dynamics

## 1 Introduction

Intraseasonal oscillation (ISO) plays an important role in the climate variability of tropical atmosphere. ISO is active over the Indo-western North Pacific (WNP) during boreal summer and has noticeable impacts on weather and climate in the Indo-western Pacific region, including the onset of

summer monsoon (Chen and Chen 1995; Wu and Wang 2001; Zhou and Chan 2005; Wu 2010; Wang et al. 2018), position and intensity of rain bands (Lau and Chan 1986; Zhu et al. 2003; Chen et al. 2015), and tropical cyclone activity (Kikuchi and Wang 2010; Huang et al. 2011). The impacts of ISO on weather and climate depend upon its intensity. Understanding the interannual variations and factors of the ISO intensity is important for the short-term climate prediction in the Indo-western Pacific region (Waliser et al. 2003; Lin 2013; Fu et al. 2013).

Over the Indo-western Pacific region, there are two prominent ISOs with different time scales: 10–20 days and 30–60 days (Chen and Chen 1993; Annamalai and Slingo 2001; Kajikawa and Yasunari 2005; Yang et al. 2008; Kikuchi and Wang 2009; Wu and Cao 2017). The 10–20-day ISO is typically originated over the equatorial western Pacific and propagates northward or northwestward to the WNP. The 30–60-day ISO is mainly originated over the equatorial Indian Ocean and propagates eastward or

✉ Renguang Wu
renguang@zju.edu.cn

1  Center for Monsoon System Research, Institute of Atmospheric Physics, Chinese Academy of Sciences, Beijing, China

2  College of Earth and Planetary Sciences, University of Chinese Academy of Sciences, Beijing, China

3  School of Earth Sciences, Zhejiang University, Hangzhou, China

4  Southern Marine Science and Engineering Guangdong Laboratory (Zhuhai), Zhuhai, China

northeastward. The 30–60-day ISO may propagate northeastward from the Maritime Continent to the WNP. Thus, both types of ISOs may have effects on the South China Sea (SCS)-WNP regions. Due to the differences in the source region and the propagation path, it is necessary to investigate the interannual variations and factors of the two types of ISOs separately. For example, Wu and Song (2018) identified notable differences in the 10–20-day and 30–60-day ISO intensity changes over the tropical WNP in El Niño-Southern Oscillation (ENSO) developing and decaying summers.

Some studies have been made on the interannual variations of the ISO intensity during boreal summer. Kim et al. (2008) obtained two major components of the interannual variations of the 20–90-day ISO intensity over the tropical Pacific and Indian Ocean during boreal summer, with the large centers in central tropical Pacific and the WNP, respectively. Similar spatial patterns were detected in the two leading empirical orthogonal function (EOF) modes of 30–90-day ISO intensity over a similar region in both winter and summer (Liu et al. 2016a). The above studies, however, did not consider or compare the differences of the two types of ISOs. Liu et al. (2016b) showed that the western North Pacific ISO is dominated by 20–40-day oscillation during the El Niño summers, but by 40–70-day oscillation during the La Niña summers. Other studies on the variations of the ISO intensity are mostly based on an intensity index defined by averaging the intensity within a certain region, like the SCS (Kajikawa and Yasunari 2005; Yang et al. 2008), the WNP (Wu and Cao 2017), or a large region over the Indo-western Pacific Ocean (Teng and Wang 2003). However, such indices may not take care of the spatial patterns of the ISO intensity changes. Thus, the specific spatial patterns of ISO intensity variations still remain unclear for the SCS-WNP region. One issue to be addressed in this study is what the spatial patterns are of the year-to-year variations of ISO intensity over the SCS-WNP region during boreal summer. A relevant issue is whether there is any difference in the interannual variations of intensity between the two types of ISOs.

The other motivation of the study is what the factors are of the year-to-year variations of ISO intensity during boreal summer. ISO intensity can be largely affected by seasonal mean atmospheric background fields over the source regions, along the propagation paths, and over the impact regions of ISO activities (Teng and Wang 2003; Kajikawa and Yasunari 2005; Liu et al. 2016a; Wu and Cao 2017). Favorable conditions for the enhanced ISO intensity include easterly vertical wind shear, low-level convergence, higher surface humidity, and anomalous ascending motions (Li and Wang 1994; Wang and Xie 1996, 1997; Maloney 2009). As the two types of ISOs have different source regions and propagation paths, the factors of the interannual variations of the intensity may be different between the two types of ISOs.

The atmospheric background fields can be modulated by sea surface temperature (SST). The important effects of ENSO on the ISO intensity variations have been identified in previous studies (Teng and Wang 2003; Liu et al. 2016a; Yang et al. 2008; Wu and Cao 2017; Wu and Song 2018). Teng and Wang (2003) noted that the westward- and northward-propagating ISOs in the WNP were enhanced in July–October during El Niño developing summer, while the northward-propagating ISOs in the Indian summer monsoon region had little linkage with ENSO. Liu et al. (2016a) pointed out that the 30–90-day ISO intensity over the central Pacific was enhanced when central Pacific SST was warmer, while the ISO intensity over the Indo-Pacific warm pool region was suppressed during eastern Pacific SST warming period. Yang et al. (2008) noted that the intensity of 12–25-day ISOs over the SCS during June–July was positively correlated with the equatorial central and eastern Pacific SST, whereas the intensity of 30–50-day ISOs was mainly linked with the western IO SST anomaly. Wu and Cao (2017) obtained similar conclusions about the SST influences on boreal summer ISO intensity over the tropical western North Pacific. They found that the 10–20-day ISO intensity was enhanced during El Niño developing summer, whereas the 30–60-day ISO intensity was enhanced during La Niña decaying summer. Therefore, the influences of ENSO differ on the two types of ISOs. Furthermore, the SST anomalies in other oceanic regions or atmospheric internal processes may affect the ISO intensity. In the present study, the factors and their influences on the ISO intensity will be investigated corresponding to different spatial patterns of 10–20-day and 30–60-day ISO intensity variations.

The aim of this study is to identify the spatial patterns and the related factors of the year-to-year variations of boreal summer 10–20-day and 30–60-day ISO intensity over the WNP. The organization of the text is as follows. Datasets and methods used in the study are described in Sect. 2. In Sect. 3, we document the spatial patterns of year-to-year variations of ISO intensity. Factors of 10–20-day and 30–60-day ISO intensity variations are presented in Sects. 4 and 5, respectively. Summary and discussions are given in Sect. 6.

## 2 Data and methods

The present study uses daily mean 850 hPa winds obtained from the National Centers for Environmental Prediction-Department of Energy (NCEP-DOE) reanalysis 2 (Kanamitsu et al. 2002). Monthly mean 850 hPa and 200 hPa winds, 500 hPa vertical p-velocity, and surface specific humidity at 2 m are also provided by NCEP-DOE reanalysis 2. The surface specific humidity is on T62 Gaussian grids and the other variables are on 2.5° × 2.5° grids for the period from January 1979 to December 2018. The

NCEP-DOE reanalysis 2 datasets are available online at ftp://ftp.cdc.noaa.gov.

Monthly mean SST data are from the NOAA optimum interpolation (OI) version 2 (Reynolds et al. 2002), provided by the NOAA/OAR/ESRL Physical Science Department (PSD), Boulder, Colorado, USA and available at http://www.esrl.noaa.gov/psd/. The NOAA Optimal Interpolation (OI) SST dataset is on a regular $1° \times 1°$ grid and covers the period from December 1981 to present.

The present study uses band-pass filtering to extract 10–20-day and 30–60-day ISOs. Following Wu (2010), 10–20-day ISOs are obtained through a 9-day running mean minus a 21-day running mean and 30–60-day ISOs are obtained through a 29-day running mean minus a 61-day running mean. The intensity of ISO within a certain period of time, such as a season, can be represented by the squared root of variance of intraseasonal variations of outgoing longwave radiation (OLR) (Salby and Hendon 1994; Kemball-Cook and Wang 2001; Liu et al. 2016a) and kinetic energy (KE) of intraseasonal variations of 850-hPa winds (Gushchina and Dewitte 2012; Wu 2018). In this study, the intensity of the ISOs is measured by the kinetic energy of intraseasonal variations of winds at 850 hPa on the 10–20-day and 30–60-day time bands, and denoted by KE1 and KE2, respectively. The average values of KE during June–July–August (JJA) represent the ISO intensity in boreal summer.

## 3 Spatial patterns of interannual variations of ISO intensity

In this section, we analyze the spatial patterns of interannual variations of the intensity of 10–20-day and 30–60-day ISOs. Before that, we first show the overall spatial distribution of interannual variations of ISO intensity. Figure 1 displays the standard deviation of interannual variations of 10–20-day and 30–60-day ISO intensity in boreal summer for the period 1979–2018.

Large mean kinetic energy of 10–20-day and 30–60-day ISOs extends from the tropical western North Pacific to the mid-latitude North Pacific (Fig. 1a, b) (Wu and Cao 2017). In comparison, the intensity of 10–20-day ISOs is larger than that of 30–60-day ISOs. Both KE1 and KE2 have the largest standard deviation over the WNP region in the tropics. The spatial distributions show notable differences between KE1 and KE2. There are three regions with large standard deviation of KE1 (Fig. 1c). One is located in the tropical WNP extending northwestward from the tropical western Pacific to the Philippines. A second one is located in the subtropical WNP. The third one lies in the mid-latitude North Pacific. Standard deviation of KE2 has two large regions (Fig. 1d). One is a zonal band along 10°–15° N with two large centers over the SCS and the Philippine Sea. The other region is located in the mid-latitude extending from south coast of Japan to the North Pacific. The present study focuses on the tropical WNP where the ISO intensity variation is most prominent among the tropical regions.
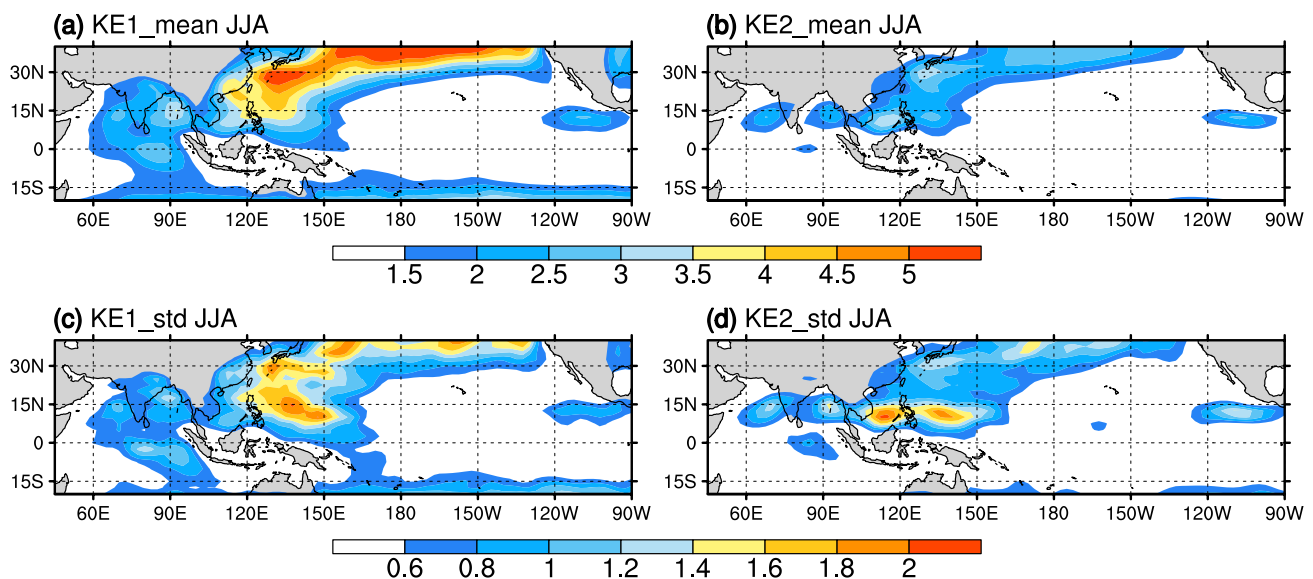


Fig. 1 Climatological mean (**a, b**) and standard deviation (**c, d**) of JJA mean kinetic energy ($m^2/s^2$) of intraseasonal winds at 850 hPa on 10–20-day (**a, c**) and 30–60-day (**b, d**) time scales for the period 1979–2018

The spatial patterns of ISO intensity variations and the corresponding time series are displayed in Fig. 2 for KE1 and in Fig. 3 for KE2. These spatial patterns are obtained by an EOF analysis applied to JJA mean KE1 and KE2 over the region 100° E–180°, 0°–30° N for the period 1979–2018. We display three EOF modes for KE1 as the percent variances of the second and third EOFs are close. For KE2, we only display the first two EOF modes. The higher modes are well separated from the leading modes according to the criterion of North et al. (1982). To confirm that the obtained EOF modes have physical meanings, we examine the distribution of KE1 and KE2 anomalies in the years with large amplitudes in the time series of principal components (PC). It turns out that the JJA mean KE1 or KE2 anomaly distributions in these years are similar to the corresponding EOF spatial patterns (figures not shown).

The first EOF mode of KE1 has large loading in a southeast-northwest tilted band (Fig. 2a), which is consistent with the large standard deviation of 10–20-day ISO intensity (Fig. 1a). The corresponding PC time series displays somewhat larger year-to-year fluctuations after than before 2000 (Fig. 2b). The second EOF mode of KE1 displays a west–east contrast distribution with positive loading extending from the Philippines to subtropics and negative loading east of 140° E (Fig. 2c). Large value of the corresponding PC time series appears in a few years, including 1986, 2000, and 2010. The third EOF mode of KE1 features a large loading region over the subtropics (Fig. 2e). This region approximately matches with the large standard deviation region over the subtropics (Fig. 1a). The corresponding PC time series appears to have higher values during the mid-1980s through the early 2000s (Fig. 2f).
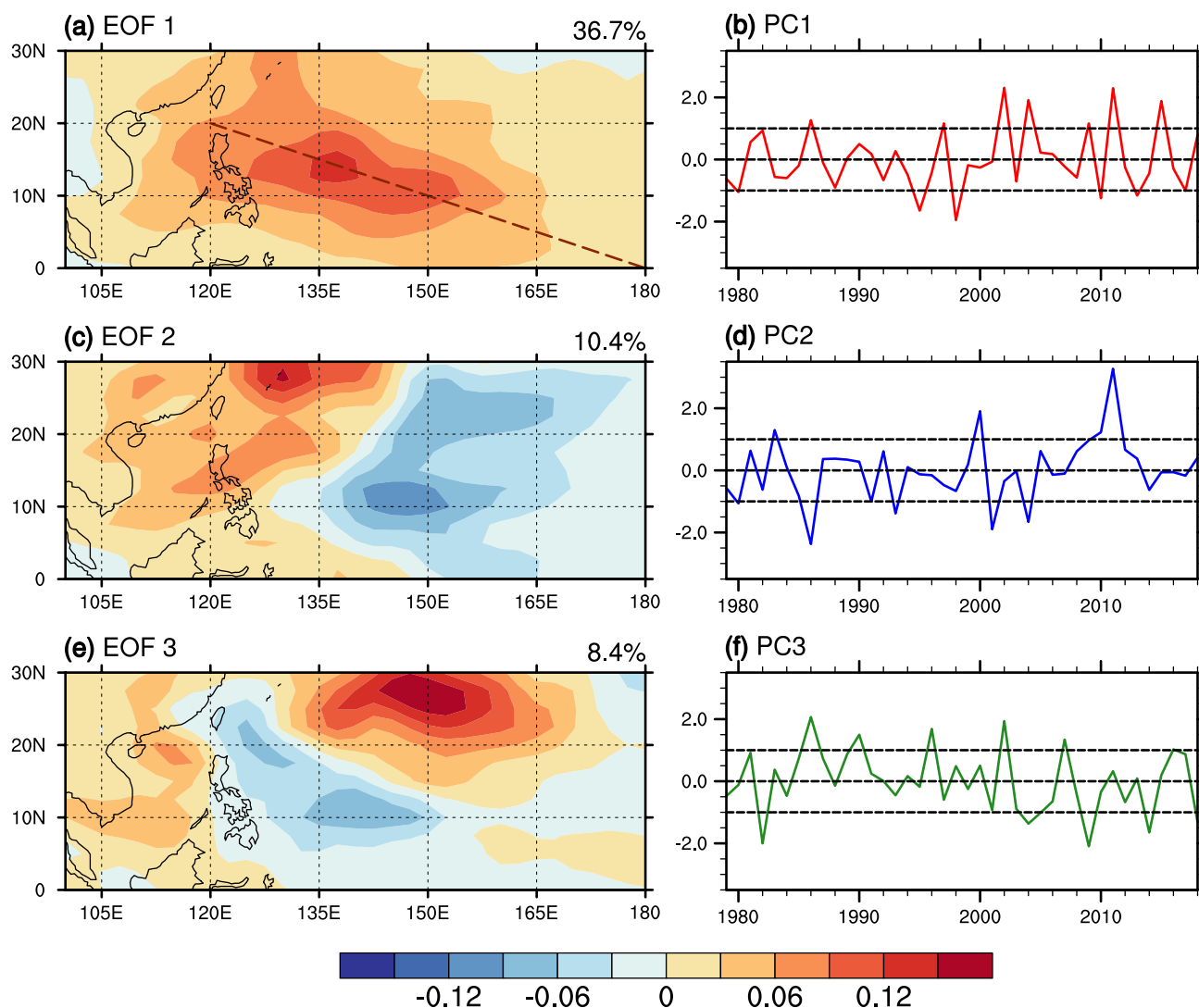


Fig. 2 Spatial patterns and time series of the three leading modes of 10–20-day ISO intensity in JJA. The three modes account for 36.7%, 10.4% and 8.4% of the variance, respectively. The dashed line in Fig. 2a denotes the section in Fig. 5
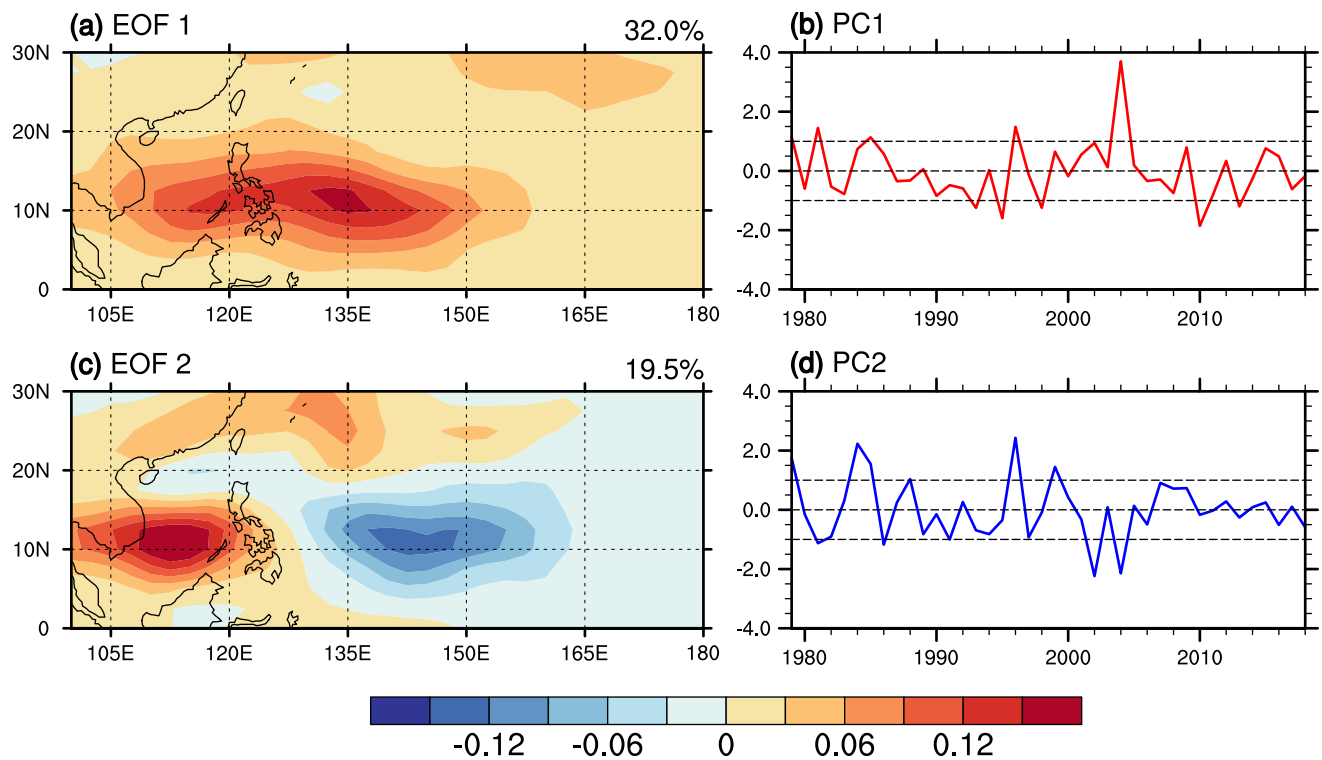
**Fig. 3** Spatial patterns and time series of the two leading modes of 30–60-day ISO intensity in JJA. The two modes account for 32.0% and 19.5% of the variance, respectively

The spatial pattern of the first EOF mode of KE2 is characterized by large loading in a zonal band extending from the SCS to the WNP along 10° N (Fig. 3a), which resembles the standard deviation of KE2 (Fig. 1b). A very large value appears in 2004 in the corresponding PC time series (Fig. 3b). A dipole pattern is observed in the spatial distribution of the second EOF mode of KE2, with a prominent contrast between the SCS and the Philippine Sea (Fig. 3c). Such a dipole pattern has been indicated in previous studies, for example, in the composite JJA mean KE2 anomalies during El Niño developing years (Wu and Song 2018, see their Fig. 5a). The year-to-year fluctuations appear relatively small after the mid-2000s in the corresponding PC time series (Fig. 3d).

Correlation coefficients between the PC time series of KE1 and KE2 are calculated to examine the relationships of 10–20-day and 30–60-day ISO intensity variations. The results are shown in Table 1. There is significant positive correlation between the first PC (PC1) of KE1 and KE2. The PC1 of KE1 and the second PC (PC2) of KE2 has a negative correlation coefficient. The relationship between these two modes is consistent with Kajikawa and Yasunari (2005) and Yang (2008) that pointed out that the intensity of quasi-biweekly and 30–50-day oscillations varied out of phase over the SCS. The PC2 of KE1 has a relatively

**Table 1** Simultaneous correlation coefficients between the three leading PCs of KE1, two leading PCs of KE2, and Niño3.4 SST in boreal summer for the period 1982–2018

|  | KE1-PC1 | KE1-PC2 | KE1-PC3 | Niño3.4 SST |
|---|---|---|---|---|
| KE2-PC1 | 0.48** | − 0.30 | − 0.01 | 0.17 |
| KE2-PC2 | − 0.43** | 0.26 | − 0.01 | − 0.37* |
| Niño3.4 SST | 0.54** | − 0.23 | − 0.13 |  |

** and * denote correlation coefficient reaching the 99% and 95% significance level, respectively

small correlation with PCs of KE2. The PC3 of KE1 has very weak correlation with PCs of KE2.

Correlations of the PCs with respect to Niño3.4 (5° S–5° N, 170° W–120° W) SST in boreal summer are also inspected as the year-to-year variations of ISO intensity in summer are shown to be related to ENSO events according to previous studies (Liu et al. 2016; Wu and Cao 2017; Wu and Song 2018). The results are included in Table 1. The correlations of PC1 of KE1 and KE2 with the Niño3.4 SST are different, significant positive for KE1 and weak positive for KE2. This is consistent with previous studies that showed a weak link of the 30–60-day ISO intensity to equatorial central-eastern Pacific SST (Teng and Wang 2003; Yang et al. 2005). The PC1 of KE1 and the PC2 of KE2 are significantly correlated with the Niño3.4 SST. The PC2 of KE1 has a

relatively small correlation with the Niño3.4 SST. The PC3 of KE1 has very weak correlation with the Niño3.4 SST.

## 4 Factors of interannual variations of 10–20-day ISO intensity

The ISO activity is modulated by seasonal mean background fields. In this section and the next section, we examine seasonal mean changes and the roles of SST anomalies to reveal the possible factors of the interannual variations of the ISO intensity. JJA mean anomalies of 850 hPa and 200 hPa wind fields, 500 hPa vertical motion, vertical shear of zonal winds, and surface specific humidity are obtained by regression on PCs of KE1 and KE2. Regressed JJA mean SST anomalies are also examined as anomalous atmospheric circulations may be induced by SST anomalies.

Corresponding to EOF1 of KE1, anomalous winds feature a lower-level cyclone and an upper-level anticyclone over the tropical WNP (Fig. 4a, b) where the year-to-year variation of KE1 is large (Fig. 1a). Anomalous ascending motion at 500 hPa, anomalous easterly vertical wind shear, and higher surface humidity cover the region extending from the Philippine Sea to the equatorial central Pacific (Fig. 4c–e). The distribution of SST anomalies shows an El Niño-like pattern, with positive anomalies in the equatorial central-eastern Pacific and negative anomalies in the WNP (Fig. 4f), which is consistent with the positive correlation between PC1 of KE1 and Niño3.4 SST (Table 1). The anomalous circulations over the WNP appear as a Rossby wave response to warmer SST in the equatorial central-eastern Pacific. The negative SST anomalies in the WNP may be attributed to the effect of seasonal mean wind and the feedback of high-frequency activity that increases upward latent heat flux (Wu 2018). Since the 10–20-day ISOs tend to originate in the equatorial central Pacific and propagates northwestward to the WNP (Yang et al. 2008), the above anomalous fields indicate that the background fields may modulate the 10–20-day ISOs
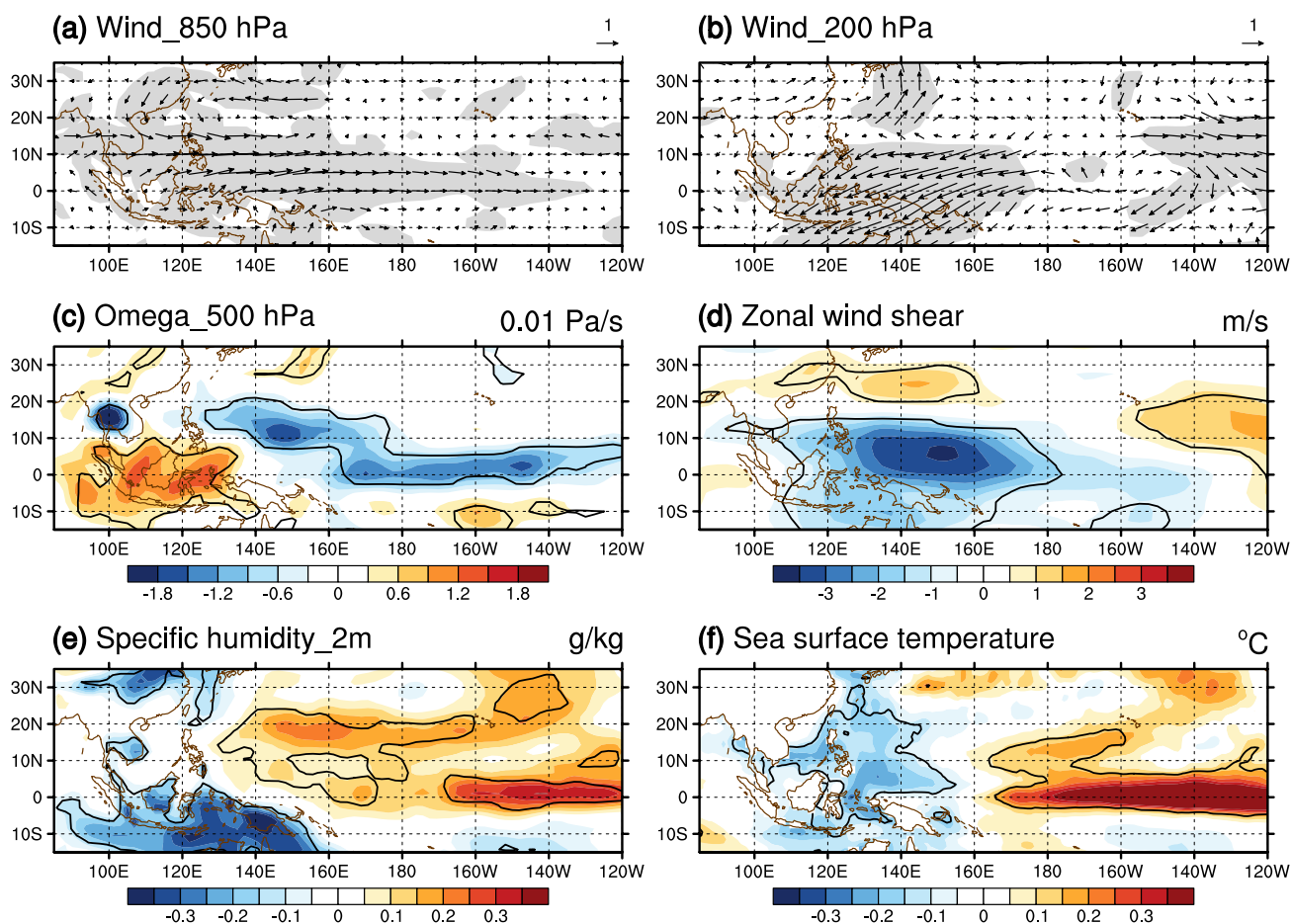


**Fig. 4** Anomalies of JJA **a** 850-hPa wind (m/s, scale at top-right), **b** 200-hPa wind (m/s, scale at top-right), **c** 500-hPa vertical p-velocity (0.01 Pa/s), **d** zonal wind difference (m/s) between 200 hPa and 850 hPa, **e** specific humidity (g/kg) at 2 m, and **f** SST (°C) obtained by regression on PC1 of 10–20-day ISO intensity. Shadings in **a**, **b** and thick lines in **c**–**f** denote that the anomalies are significant at the 95% confidence level according to the Student t test. The analysis time period is 1979–2018 in **a**–**e** and is 1982-2018 in **f**

both in the source region and along the propagation path and thus the seasonal mean 10–20-day ISO intensity over the WNP.
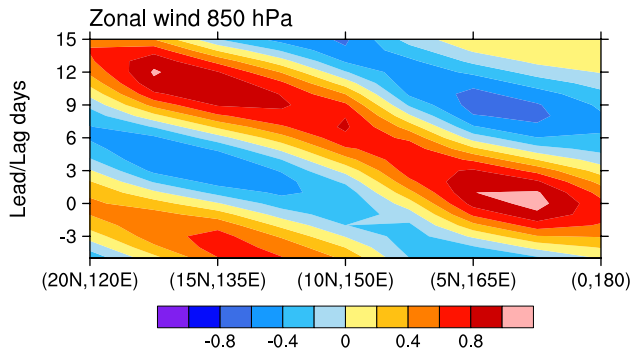


**Fig. 5** Lead-lag regression of 850-hPa zonal wind (m/s) along the section from 20° N, 120° E to 0°, 180° (the dashed line in Fig. 2a) with respect to area-mean 10–20-day 850-hPa zonal winds averaged over the region of 2.5° S–2.5° N and 160° E–180° for the period June 10th to August 21st in 1982, 1986, 1997, 2002, 2004, 2009, 2011, and 2015

To illustrate the northwestward propagation of 10–20-day ISOs, we examine the lead-lag intraseasonal perturbations of 850-hPa winds, which are obtained by regression on area-mean 10–20-day filtered 850-hPa zonal winds over the equatorial central Pacific (2.5° S–2.5° N, 160° E–180°) during the years with large PC1 of KE1. As shown in Fig. 5 that displays 850-hPa zonal wind perturbations along a section from 20° N, 120° E to 0°, 180° (denoted by the dashed line on Fig. 2a), 10–20-day ISO signals propagate northwestward from the equatorial central Pacific to the WNP.

Corresponding to EOF2 of KE1, there are lower-level easterly and upper-level westerly wind anomalies over the tropical central-western Pacific (Fig. 6a, b), leading to strong anomalous westerly wind shear (Fig. 6d) that suppresses ISO activities there. The anomalous ascending motion east of Taiwan (Fig. 6c) is favorable for enhanced ISO activities over the subtropical WNP. We note that the vertical shear has little effect on the ISO intensity change in the positive loading region and the vertical motion cannot explain the ISO intensity change near the Philippines and in the negative loading region. Specific humidity anomalies are small
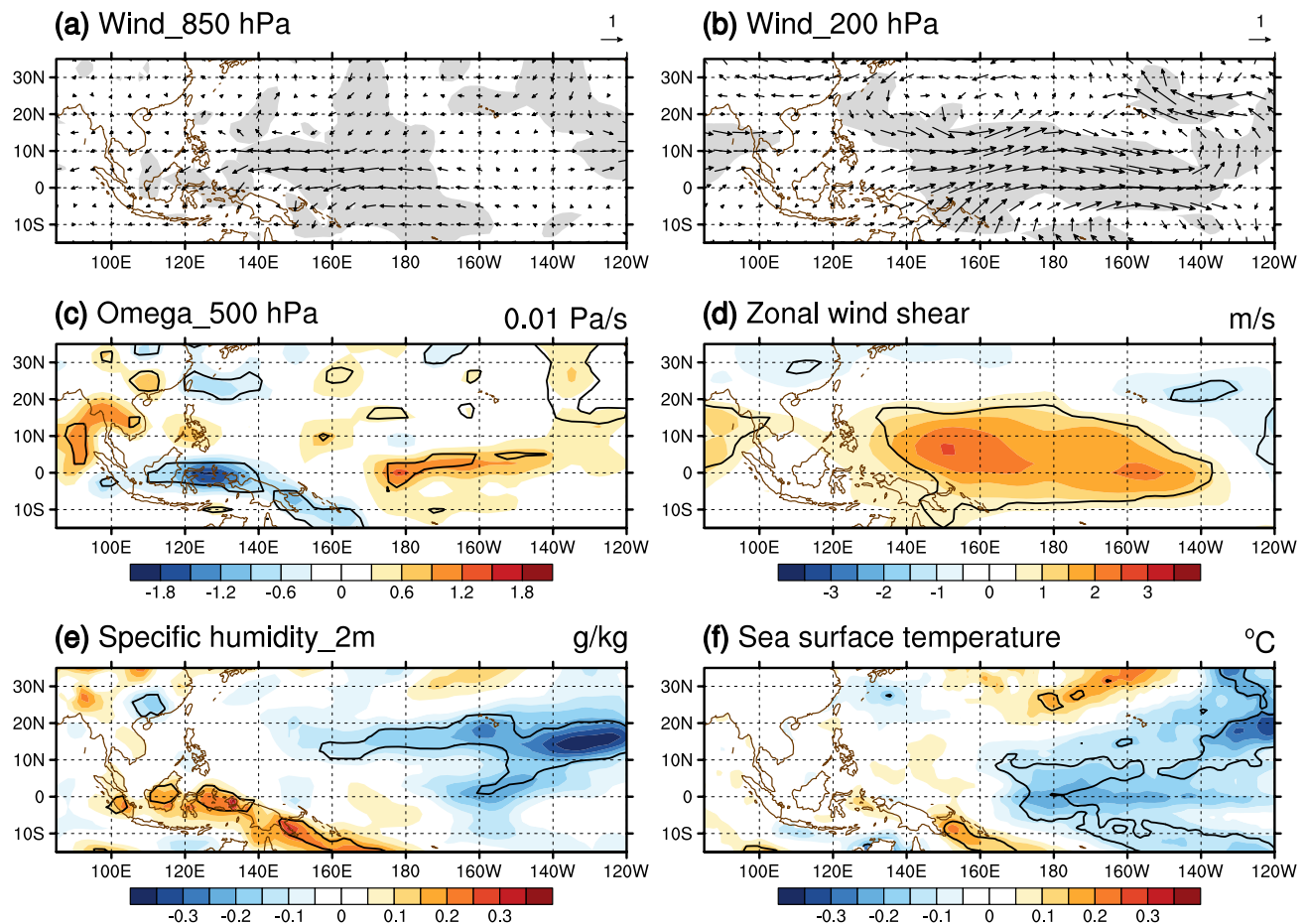


**Fig. 6** The same as Fig. 4 except with respect to PC2 of 10–20-day ISO intensity

west of 140° E (Fig. 6e), indicative of little effect on EOF2 of KE1. Thus, the signal in environmental variables is not so obvious. Negative SST anomalies are observed in the tropical central-eastern Pacific (Fig. 6f), which may explain anomalous winds over the tropical WNP via a Rossby wave response.

The anomalous ascending motion east of Taiwan may be remotely induced by the equatorial central-eastern Pacific SST anomalies. Negative velocity potential and divergent winds at 850-hPa as well as positive velocity potential and convergent winds at 200-hPa are observed over the tropical central-eastern Pacific (Fig. 7), which may be attributed to negative SST anomalies in the equatorial central-eastern Pacific (Fig. 6f). Westward lower-level divergent winds split into two branches, leading to convergence over the Maritime Continent and the region east of Taiwan separately (Fig. 7a). Opposite divergent winds are observed at upper-level (Fig. 7b). The lower-level convergence and upper-level divergence induce anomalous ascending motion over the subtropical WNP (Fig. 6c), enhancing the ISO intensity there.

Above analysis shows that both the first and second EOF modes of KE1 are related to the equatorial central-eastern Pacific SST anomalies. Here, we compare the lead-lag
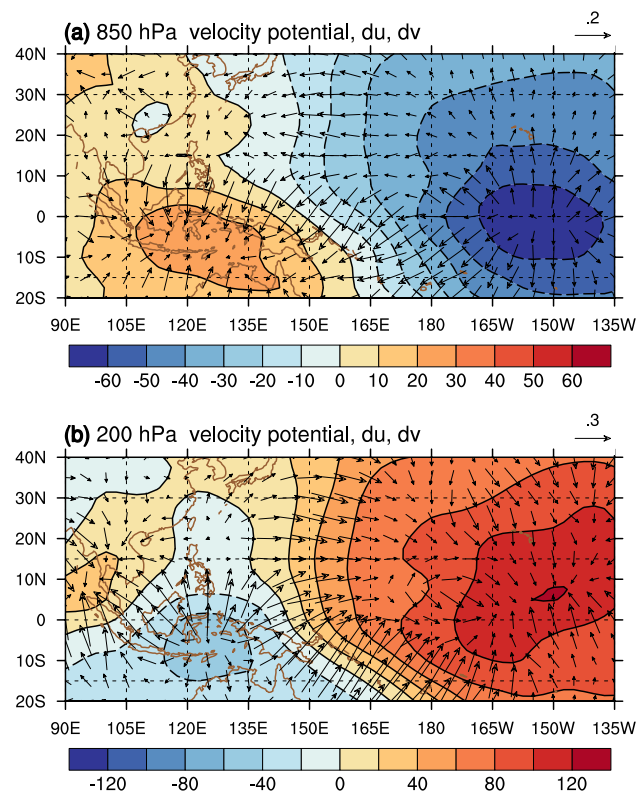
correlation of PC1 and PC2 with the Niño3.4 SST to inspect the influence of ENSO events. A very similar lead-lag correlation is obtained with the Niño4 SST. The correlation coefficient between PC1 and Niño3.4 SST is significant from simultaneous summer to the next spring (Fig. 8). This indicates that ISO intensity associated with the EOF1 of KE1 is enhanced (suppressed) during the developing stage of El Niño (La Niña) events, which is consistent with Wu and Cao (2017). The ISO intensity associated with the EOF2 of KE1 subjects to change in the ENSO developing stages as well, but with a relatively weak correlation with simultaneous Niño3.4 SST.

The differences in the distribution of environmental changes between EOF1 and EOF2 of KE1 indicate a difference manner of equatorial central-eastern Pacific SST anomalies. For EOF1 mode, the influence of the equatorial central-eastern Pacific SST anomalies is directly via a northwestward extending Rossby wave type response that affects both the source region and the propagation path of the 10–20-day ISOs. For EOF2 mode, the influence of the equatorial central-eastern Pacific SST anomalies includes a direct Rossby wave type response that affects the eastern part and an indirect way by large-scale divergent circulation that affects the western part. The direct influence is weaker compared to the EOF1 mode due to smaller SST anomalies. The above differences may be related to the different distribution and magnitude of equatorial central-eastern Pacific SST anomalies. The SST anomalies corresponding to the PC1 are larger and have a wider zonal extent and those corresponding to the PC2 are weaker and shift westward.

Corresponding to the EOF3 of KE1, no significant signals have been identified based on a regression analysis with respect to PC3 (figure not shown). This indicates that the signal for EOF3 mode is not obvious, which is expected as the percent variance explained by this mode is not high. Here, we perform a composite analysis based on area-mean KE1 over the region of 20°–30° N, 140°–160° E. We select 9 positive area-mean KE1 years (1981, 1985, 1986, 1989,



Fig. 7 JJA mean velocity potential (shadings, $1 \times 10^4$ s$^{-1}$) and divergent wind (vectors, m/s, scale at top-right) at **a** 850 hPa and **b** 200 hPa regressed on PC2 of KE1
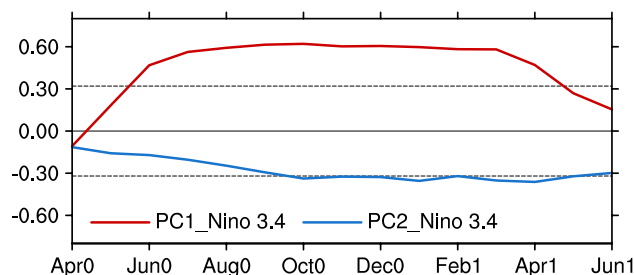


Fig. 8 Correlation of monthly mean Niño3.4 SST from April to June of the following year with respect to PC1 (red line) and PC2 (blue line) of KE1 in JJA. "0" after the season denotes the same year as KE1 and "1" denotes the following year. The dashed horizontal lines denote the 95% confidence level

1990, 1996, 2007, 2016, and 2017) and 9 negative area-mean KE1 years (1979, 1982, 1992, 1995, 1997, 2003, 2005, 2013, and 2014) during which the magnitude of area-mean KE1 is larger than one 0.5 standard deviation. We reverse the anomalies in negative area-mean KE1 years and combine them with those in positive area-mean KE1 years when constructing the composite. The composite KE1 reaches 1 m²/s² in the reference region (Fig. 9a). The KE1 increase co-locates with an anomalous lower-level cyclone (Fig. 9b) and anomalous upward motion to southeast (Fig. 9c). The spatial relation of lower-level cyclone and vertical motion distribution suggests a positive atmospheric circulation-heating feedback. The enhanced upward motion leads to condensation of water vapor and latent heat release that induces a lower-level cyclone located to the northwest as a Rossby wave response. In turn, anomalous lower-level winds cause moisture convergence and contribute to upward motion. Weak negative SST anomalies are obtained in the region (Fig. 9d), which is likely a result of seasonal mean anomaly and enhanced KE1 (Wu 2018).

Notable negative SST anomalies are seen in the equatorial central-eastern Pacific (Fig. 9d), accompanied by anomalous downward motion (Fig. 9c) and anomalous lower-level easterlies to the west (Fig. 9b). This suggests an influence of the equatorial central-eastern Pacific SST anomalies. This influence is likely through large-scale divergent flows. This is confirmed by composite velocity potential anomalies

and associated divergent winds (Fig. 10). There are anomalous upper-level convergence, lower-level divergence, and
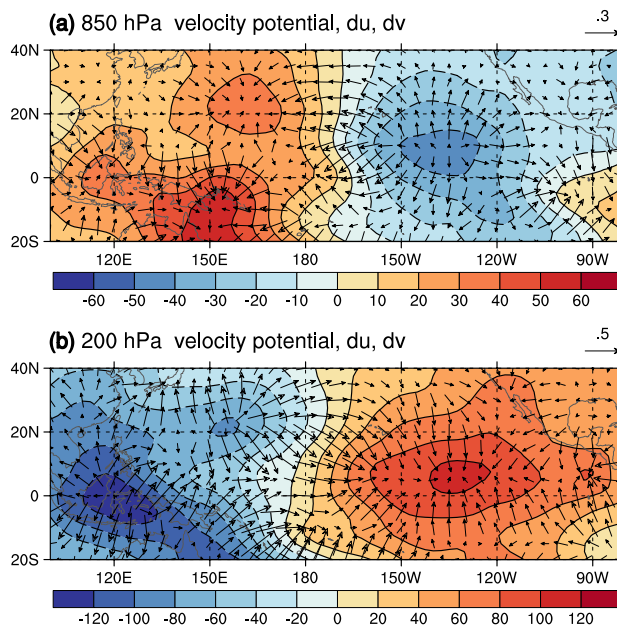


**Fig. 10** Composite anomalies of JJA velocity potential (shadings, $1 \times 10^4$ s$^{-1}$) and divergent wind (vectors, m/s, scale at top-right) at **a** 850 hPa and **b** 200 hPa based on area-mean 10–20-day ISO intensity in the region of 20°–30° N, 140°–160° E
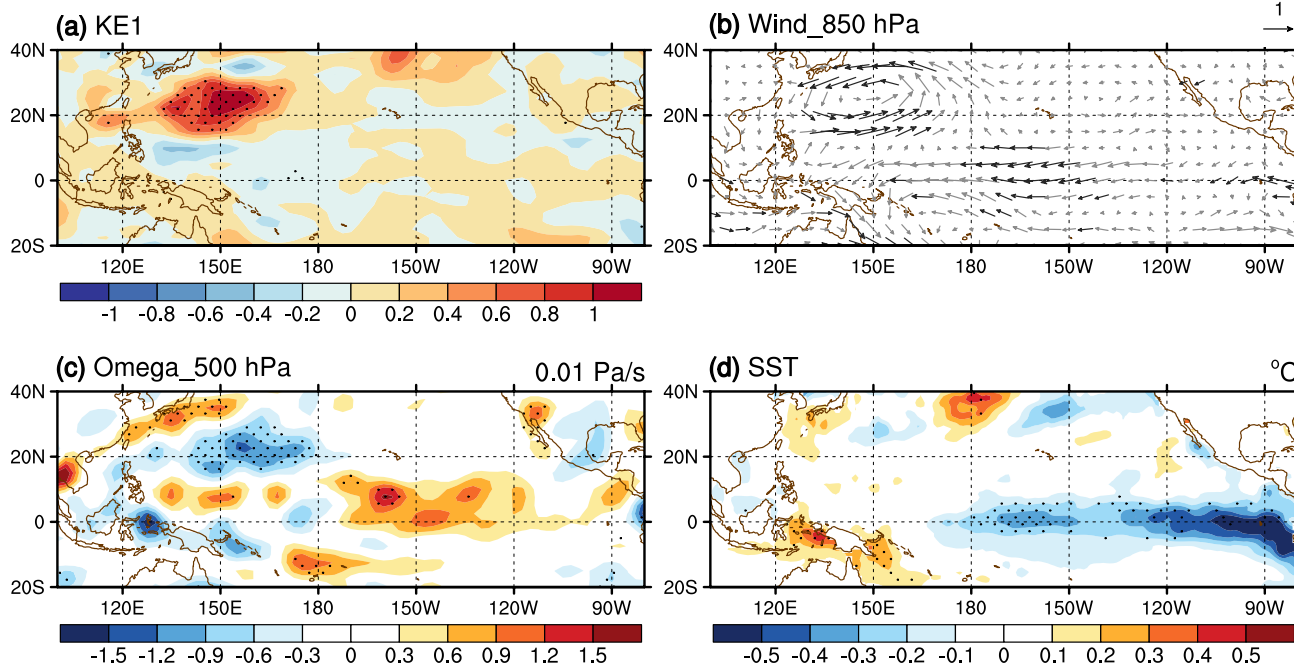


**Fig. 9** Composite anomalies of JJA **a** 10–20-day kinetic energy (m²/s²), **b** 850-hPa wind (m/s, scale at top-tight), **c** 500-hPa vertical p-velocity (0.01 Pa/s), and **d** SST (°C) based on area-mean 10–20-day ISO intensity in the region of 20°–30° N, 140°–160° E. Bold vectors and dotted regions denote anomalies significant at the 95% confidence level

downward motion over the equatorial eastern Pacific. Anomalous upper-level divergence, lower-level convergence, and upward motion are observed over the subtropical western North Pacific, which favors intensified ISOs.

## 5 Factors of interannual variations of 30–60-day ISO intensity

Corresponding to the EOF1 of KE2, an anomalous lower-level cyclone and an anomalous upper-level anticyclone are observed over the tropical WNP (Fig. 11a, b). The associated anomalous ascending motion and easterly vertical wind shear (Fig. 11c, d) contribute to the intensification of ISOs. The moisture anomalies are small over most of the WNP (Fig. 11e). The above background field changes can be attributed to effects of both tropical North Indian Ocean (NIO) and central North Pacific Ocean (NPO) SST anomalies (Fig. 11f). The Kelvin wave response to negative NIO SST anomalies and the Rossby wave response to positive NPO SST anomalies work together to induce anomalous

lower-level cyclone and upper-level anticyclone over the WNP (He and Wu 2014; Wu et al. 2014).

A question is what the relative contributions are of NIO and NPO SST anomalies to anomalous circulations over the WNP. To address this question, we calculate the correlation coefficients of area-mean SST anomalies in the NIO (10°–20° N, 60°–100° E) and NPO (10°–20° N, 150° E–170° W) with PC1 of KE2. The correlation coefficient of NIO SST (− 0.41) is somewhat larger than that of NPO SST (0.31). The above two correlation coefficients are both significant at the 95% confidence level. It is worth noting that the correlation coefficient between NIO and NPO SST is only − 0.08. Figure 12 compares the composite KE2 anomalies and the corresponding background fields in the years when there are large SST anomalies in NIO and NPO individually or in both regions with opposite signs. Here, the years are determined based on a 0.5 standard deviation of SST anomalies. We reverse the anomalies in negative PC2 years and combine them with those in positive PC2 years in the construction of the composite. When NIO SST is cooler and NPO SST is normal, KE2 is mainly enhanced
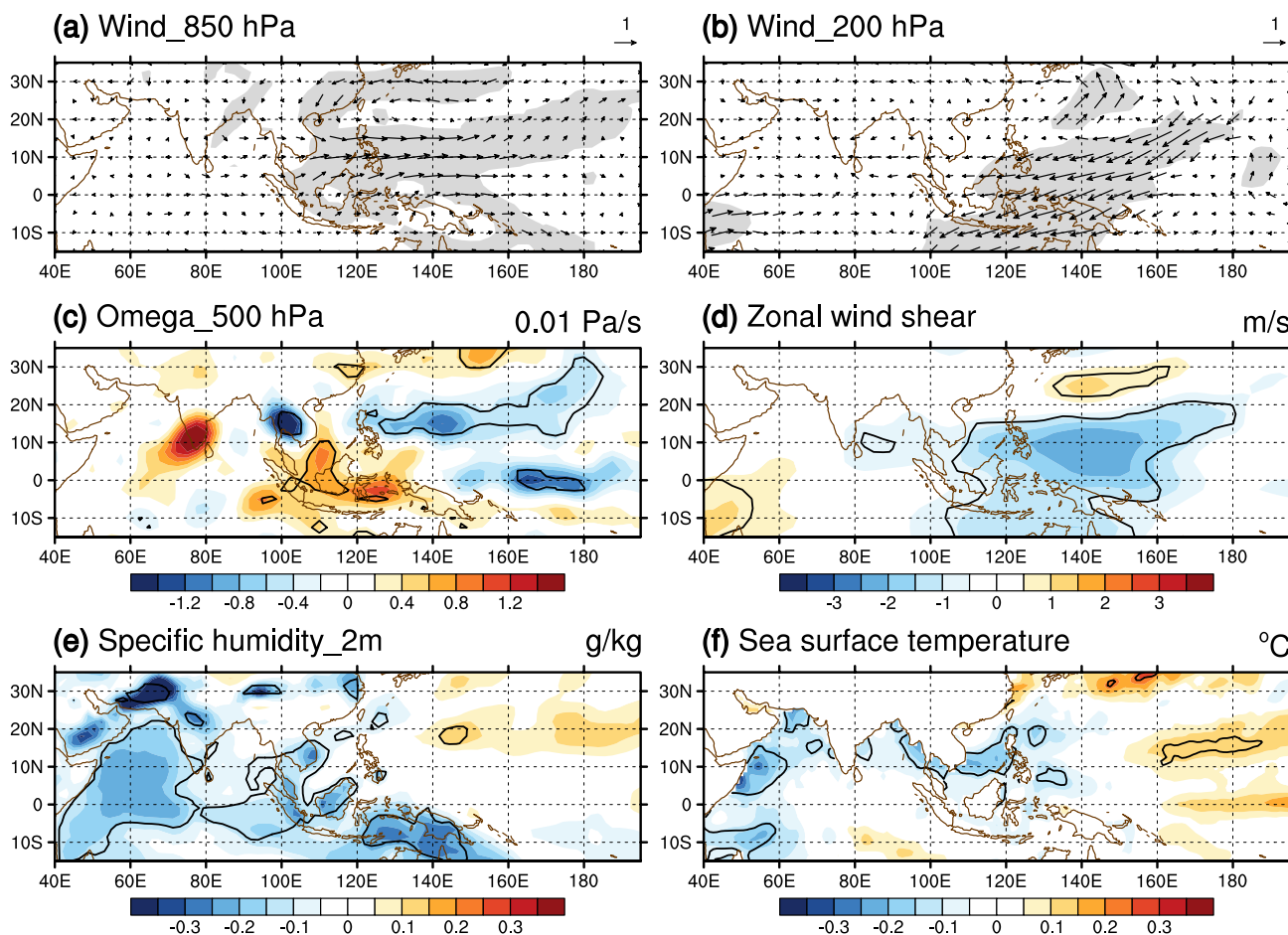


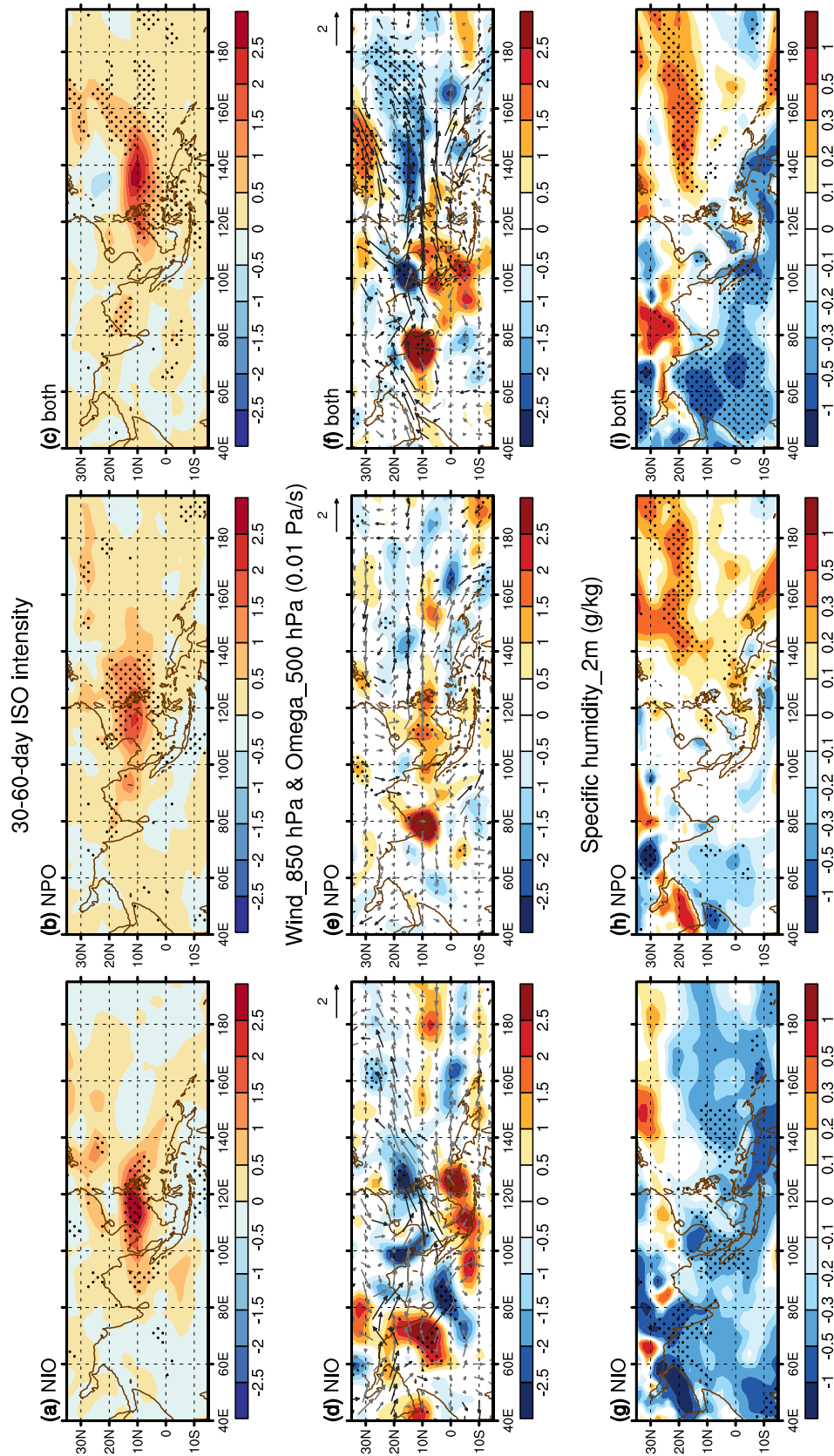**Fig. 11** The same as Fig. 4 except with respect to PC1 of 30–60-day ISO intensity

**Fig. 12** Composite anomalies of 30–60-day kinetic energy (m²/s²), 850-hPa wind (m/s, scale at top-right), 500-hPa vertical p-velocity (0.01 Pa/s), and 2-m specific humidity (g/kg) in the years when the standardized **a, d, g** PC1-KE2>0.5, NIO SST>0.5, NPO ISSTI<0.5, or PC1-KE2<−0.5, NIO SST<−0.5, NPO ISSTI>0.5, NIO ISSTI<0.5, or PC1-KE2<−0.5, NPO SST<−0.5, NIO ISSTI<0.5, and **c, f, i** PC1-KE2>0.5, NIO SST>0.5, NPO SST>0.5, NIO SST>0.5, NPO SST<−0.5. Bold vectors and dotted regions denote anomalies significant at the 90% confidence level

$\textcircled{2}$ Springer

over the SCS (Fig. 12a). The anomalous lower-level westerly winds induced by negative NIO SST anomalies converge to the SCS and cause anomalous ascending motion there (Fig. 12d). Surface specific humidity anomalies are small over the SCS and the Philippine Sea (Fig. 12g). When NPO SST is warmer and NIO SST is normal, enhanced KE2 extends from the SCS to the Philippine Sea (Fig. 12b). The Rossby wave response to the warmer NPO SST features a lower-level anomalous cyclone over the tropical WNP (Fig. 12e). The associated anomalous easterly vertical wind shear covers the SCS and the Philippine Sea, contributing to the enhancement of 30–60-day ISO intensity there. Vertical motion and surface humidity have weak anomalies over the ocean east of the Philippines (Fig. 12e, h). Anomalous descending motion is observed over the SCS (Fig. 12e). When the cooler NIO and warmer NPO appear together, the intensified KE2 covers the SCS and the tropical WNP (Fig. 12c). Significant lower-level easterly wind anomalies extend from the SCS to the tropical WNP Pacific along with anomalous ascending motion and higher humidity over the tropical WNP (Fig. 12f, i), enhancing 30–60-day ISO

intensity there (Fig. 12c). The above comparison suggests that the negative NIO SST anomalies enhance the 30–60-day ISO intensity over the SCS mainly via dynamical process and positive NPO SST anomalies enhance the 30–60-day ISO intensity over the SCS and the Philippine Sea via both dynamical and thermodynamical processes.

The regressed background fields corresponding to EOF2 of KE2 are somewhat similar to those associated with EOF1 of KE1. Anomalous lower-level anticyclone and upper-level cyclone are observed over the tropical WNP (Fig. 13a, b) in response to lower SST in the equatorial central Pacific (Fig. 13f). Consequently, anomalous descending motion and anomalous westerly vertical shear, and lower specific humidity appear over the tropical WNP (Fig. 13c–e), suppressing the 30–60-day ISO activity. In comparison, anomalous atmospheric fields shift eastward compared to those associated with EOF1 of KE1 (Fig. 4a). Anomalous ascending motion and higher humidity are observed over the Maritime Continent (Fig. 13c, e), consistent with anomalous lower-level convergence and upper-level divergence (Fig. 13a, b). These changes may be attributed to a remote impact of
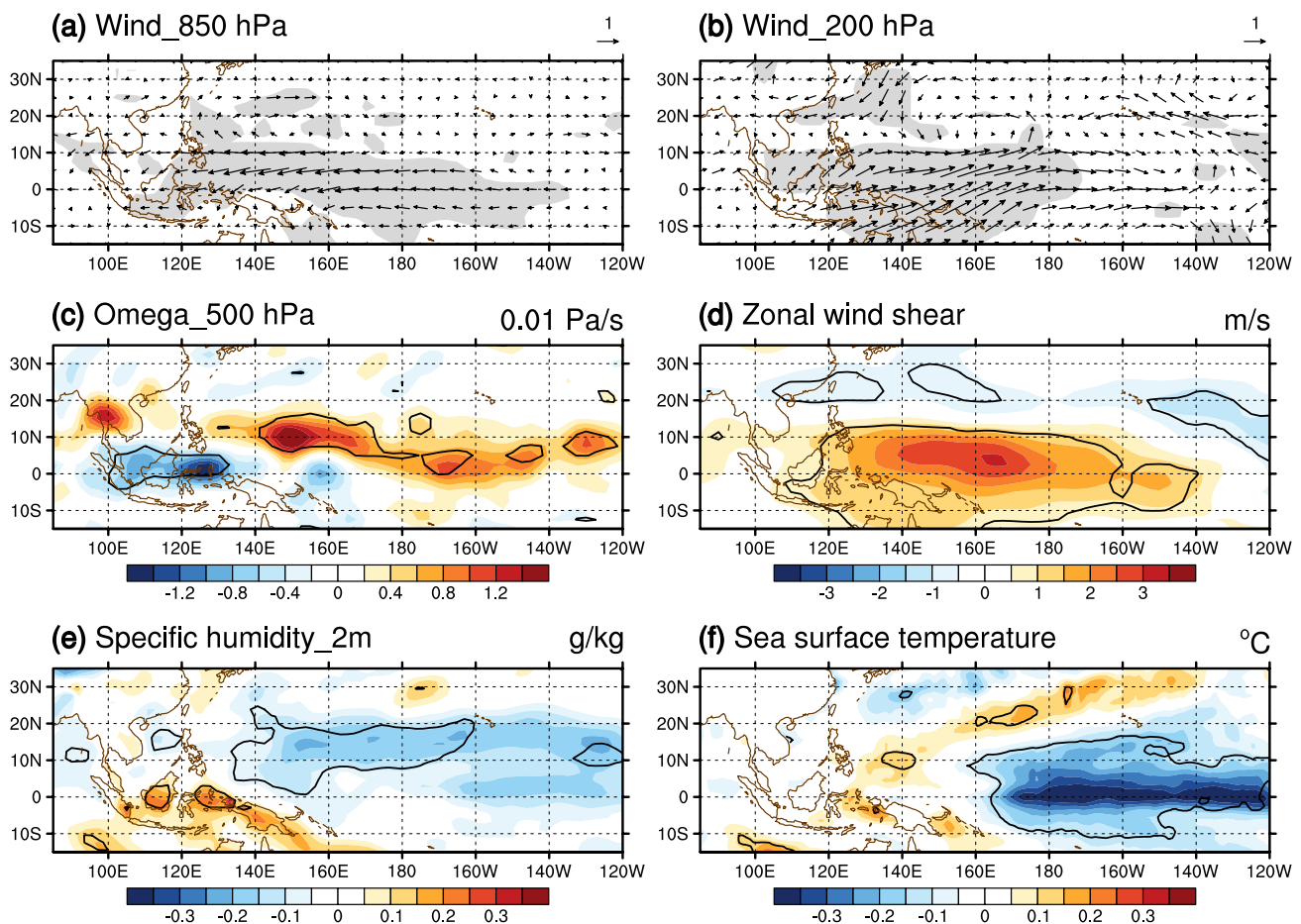


**Fig. 13** The same as Fig. 4 except with respect to PC2 of 30–60-day ISO intensity

negative SST anomalies in the equatorial central Pacific (Fig. 13f) via an anomalous Walker circulation. The above atmospheric changes enhance the 30–60-day ISO activity over the Maritime Continent that is a source region of northeastward propagating 30–60-day ISOs (Yang et al. 2008). In turn, an intensification of 30–60-day ISOs occurs over the SCS region when these ISOs arrive there. The northward propagation of 30–60-day ISOs is illustrated by the temporal evolution of 30–60-day OLR anomalies along 105°–125° E obtained by regression with respect to area-mean 30–60-day OLR anomalies in the region of 2.5° S–2.5° N, 107.5°–112.5° E (Fig. 14). The regression is based on the 7 the years (1979, 1984, 1985, 1988, 1996, 1999, and 2007) when the PC2 of KE2 is large positive (Fig. 3d). It is obvious that the 30–60-day OLR signals propagate northward from the Maritime Continent to the northern SCS.

Here, we compare the relationship of EOF1 and EOF2 modes of KE2 with the Niño3.4 SST. The correlation of PC1 of KE2 and Niño3.4 SST is negative during the preceding winter to spring and positive in the following fall (Fig. 15a). This indicates that the SCS-WNP KE2 tends to be enhanced during the decaying summer of La Niña events or the developing summer of El Niño events or during the transition from La Niña to El Niño. Significant negative correlation of PC2 and Niño3.4 SST lasts from spring to winter (Fig. 15a). This suggests that opposite KE2 changes tend to occur over the SCS and WNP during developing El Niño and La Niña events.
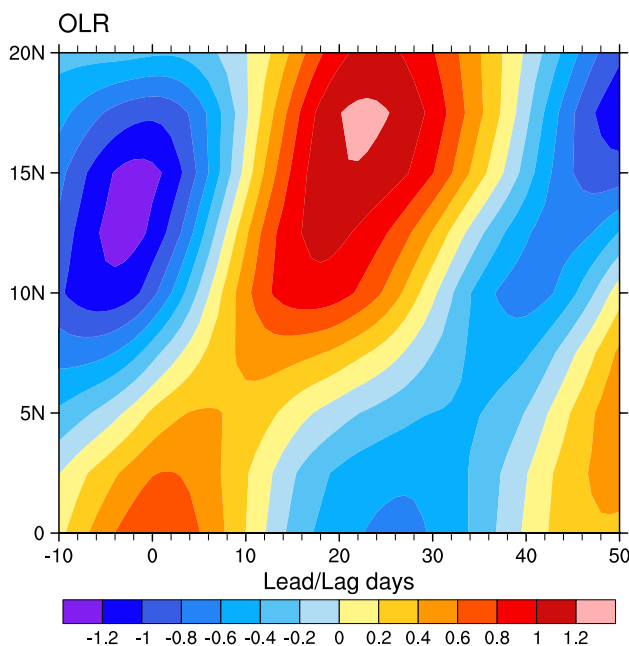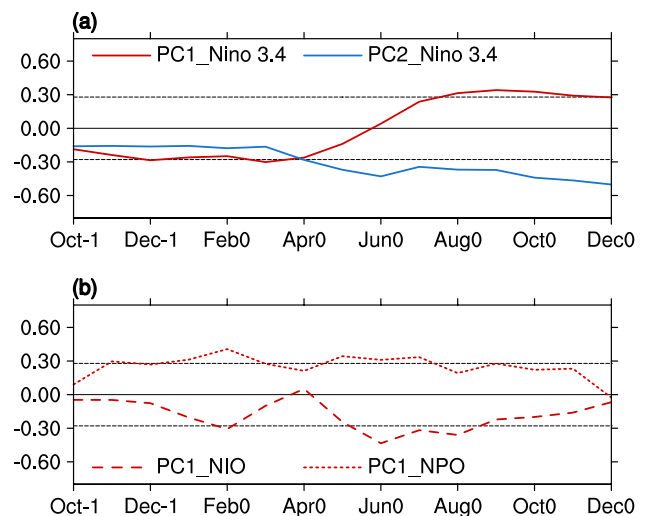


**Fig. 15** Correlation of **a** monthly mean Niño 3.4 SST from April to June of the following year with respect to PC1-KE2 (red solid line) and PC2-KE2 (blue solid line) in JJA and **b** monthly mean NIO SST (red long dashed line) and NPO SST (red short dashed line) from April to June of the following year with respect to PC1-KE2. "0" after the season denotes the same year as KE2 and "−1" denotes the preceding year. The dashed horizontal lines denote the 90% confidence level

The combined effects of NIO and NPO SST anomalies on EOF1 of KE2 are confirmed by their lead-lag correlation with PC1 of KE2 (Fig. 15b). According to previous studies (Klein et al. 1999; Du et al. 2009), preceding La Niña events are followed by SST decrease in the NIO in the following summer. At the same time, the NPO SST anomalies tend to be positive in the La Niña decaying stage. As such, the above regional SST effects partly indicate an indirect impact of ENSO on KE2 over the SCS-WNP.

## 6 Summary and discussions

The present study analyzes the spatial patterns and factors of year-to-year variations of 10–20-day and 30–60-day ISO intensity in boreal summer over the tropical WNP. For 10–20-day ISO intensity variation, the first EOF mode has large loading in a southeast-northwest tilted band over the WNP. The second EOF mode shows a southeast–northwest contrast between the tropical and subtropical WNP. The third mode shows large loading over the subtropical WNP. For 30–60-day ISO intensity, the first EOF mode has large loading in a west–east oriented band over the SCS and the WNP. The second EOF mode shows an east–west dipole pattern with a contrast between the SCS and the Philippine Sea.

Analysis shows that tropical Indo-Pacific SST anomalies modulate the ISO intensity over the tropical WNP through modulating seasonal mean background fields. The impacts



**Fig. 14** 30–60-day OLR anomalies (W/m$^2$) along 105°–125° E obtained by regression with respect to area-mean 30–60-day OLR anomalies in the region of 2.5° S–2.5° N, 107.5°–112.5° E based on the years 1979, 1984, 1985, 1988, 1996, 1999, and 2007

of the SST anomalies on the ISO intensity can be summarized into three types. The first type is a direct influence of ENSO. This type of impacts is obvious on the first mode of 10–20-day ISO intensity variation and the eastern portion of the second mode of both 10–20-day and 30–60-day ISO intensity variation (Fig. 16a, b, d). During the developing ENSO events, the equatorial central-eastern Pacific SST anomalies modulate seasonal mean fields via a Rossby wave type response over the tropical WNP, and thus influence the ISO activity there (Fig. 16a). This type of influence is most prominent on the first mode of 10–20-day ISO intensity change as seasonal mean fields are largely modulated both in the source region and along the propagation path of northwestward propagating 10–20-day ISOs.

The second type is an indirect influence of ENSO. This type of impacts is obvious on the western portion of the second mode of both 10–20-day and 30–60-day ISO intensity variation (Fig. 16b, d) as well as the third mode of 10–20-day ISO intensity variation. In this type, the equatorial central-eastern Pacific SST anomalies modulate seasonal mean fields over the subtropical WNP and the Maritime Continent via an anomalous Walker circulation and related anomalous divergence and convergence. For the second mode of 10–20-day ISO intensity variation, the seasonal mean changes in the eastern portion and the western portion have an opposite effect, leading to a northwest–southeast contrasting pattern. For the second mode of 30–60-day ISO intensity variation, the modified seasonal mean fields over the Maritime Continent affects the intensity of northward propagating ISOs that reach the SCS (Fig. 16d). Due to the opposite effect of

seasonal mean changes between the Maritime Continent and the tropical WNP, a west–east contrasting pattern is induced in the ISO intensity change.

The third type is impacts of SST anomalies outside of the equatorial central-eastern Pacific. This type of influence is prominent on the leading mode of 30–60-day ISO intensity (Fig. 16c). During the ENSO decaying stage, opposite SST anomalies in NIO and NPO excite Kelvin-wave and Rossby-wave type circulation anomalies, respectively. Together, they modulate seasonal mean fields over the SCS and tropical WNP and thus the 30–60-day ISO intensity. The NIO SST anomalies mainly influence the 30–60-day ISO intensity over the SCS, and KE2 anomalies extend more eastward when SST anomalies are present in the NPO.

In addition to the role of SST anomalies, the internal atmospheric process may play a role in the 10–20-day ISO intensity change over the subtropical WNP. In this region, a positive feedback between circulation and heating appears to modulate the seasonal mean background fields that in turn affect the 10–20-day ISO intensity. The positive circulation-heating feedback may also work for the 10–20-day ISO intensity change over the tropical WNP.

The present study focuses on roles of seasonal mean SST anomalies in the year-to-year variations of the ISO intensity. An issue worthy of investigation is whether the ISO intensity change can have a feedback on seasonal mean SST by modulating surface heat fluxes (Wu 2018). A relevant issue is which type of ISO intensity anomaly pattern is more effective in the upscale feedback. We will address these issues in future studies.
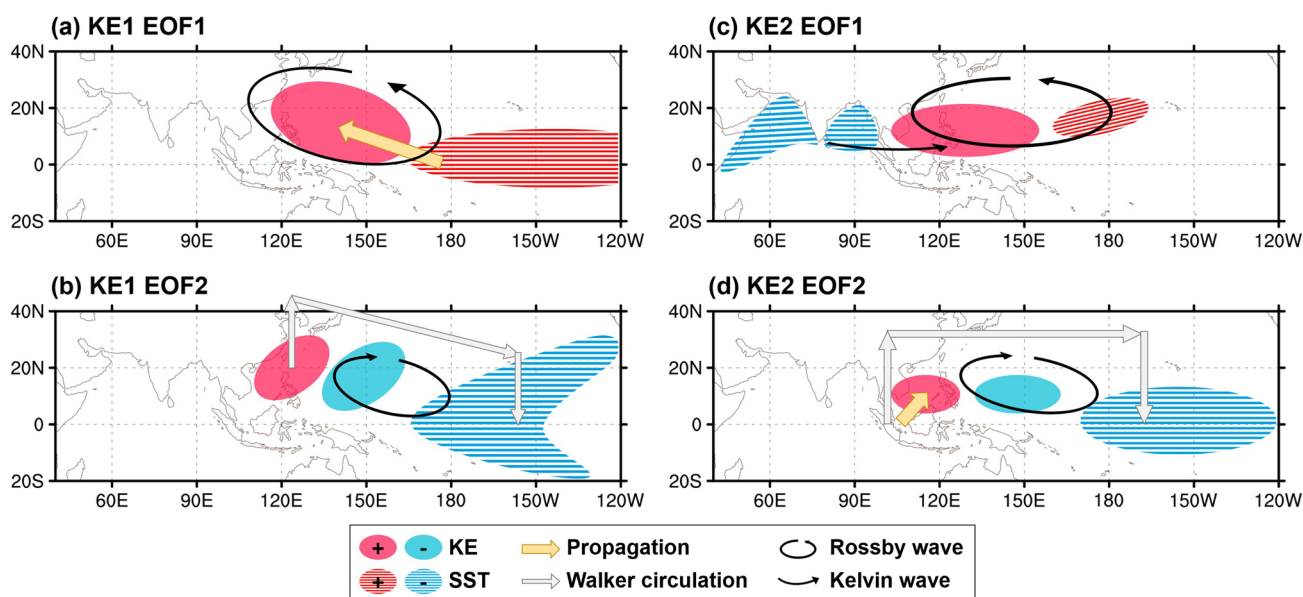


**Fig. 16** Schematic diagram for intensity variation of **a** EOF1 and **b** EOF2 mode of 10–20-day ISO and **c** EOF1 and **d** EOF2 mode of 30–60-day ISO

# References

Annamalai H, Slingo JM (2001) Active/break cycles: diagnosis of the intraseasonal variability of the Asian summer monsoon. Clim Dyn 18:85–102

Chen TC, Chen JM (1993) The 10–20-day mode of the 1979 Indian monsoon: Its relation with the time variation of monsoon rainfall. Mon Weather Rev 121:2465–2482

Chen TC, Chen JM (1995) An observational study of the South China Sea monsoon during the 1979 summer: onset and life cycle. Mon Weather Rev 123:2295–2318

Chen JP, Wen ZP, Wu R, Chen ZS, Zhao P (2015) Influences of northward propagating 25–90-day and quasi-biweekly oscillations on eastern China summer rainfall. Clim Dyn 45(102):105–124

Du Y, Xie SP, Huang G, Hu K (2009) Role of air-sea interaction in the long persistence of El Niño-induced North Indian Ocean warming. J Clim 22:2023–2038

Fu XH, Lee JY, Wang B, Wang WQ, Vitart F (2013) Intraseasonal forecasting of the Asian summer monsoon in four operational and research models. J Clim 26:4186–4203

Gushchina D, Dewitte B (2012) Intraseasonal tropical atmospheric variability associated with the two favors of El Niño. Mon Weather Rev 140:3669–3681

He Z, Wu R (2014) Indo-Pacific remote forcing in summer rainfall variability over the South China Sea. Clim Dyn 42(9):2323–2337

Huang P, Chou C, Huang R (2011) Seasonal modulation of tropical intraseasonal oscillations on tropical cyclone geneses in the western North Pacific. J Clim 24(24):6339–6352

Kajikawa Y, Yasunari T (2005) Interannual variability of the 10–25- and 30–60-day variation over the South China Sea during boreal summer. Geophys Res Lett 32:L04710. https://doi.org/10.1029/2004GL021836

Kanamitsu M, Ebisuzaki W, Woollen J, Yang SK, Hnilo JJ, Fiorino M, Potter GL (2002) NCEP–DOE AMIP-II reanalysis (R-2). Bull Am Meteorol Soc 83:1631–1643

Kemball-Cook S, Wang B (2001) Equatorial waves and air–sea interaction in the boreal summer intraseasonal oscillation. J Clim 14:2923–2942

Kikuchi K, Wang B (2009) Global perspective of the quasi-biweekly oscillation. J Clim 22:1340–1359

Kikuchi K, Wang B (2010) Formation of tropical cyclones in the northern Indian Ocean associated with two types of tropical intraseasonal oscillation modes. J Meteorol Soc Jpn 88:475–496

Kim HM, Kang IS, Wang B, Lee JY (2008) Interannual variations of the boreal summer intraseasonal variability predicted by ten atmosphere–ocean coupled models. Clim Dyn 30(5):485–496

Klein SA, Soden BJ, Lau NC (1999) Remote sea surface temperature variations during ENSO: evidence for a tropical atmospheric bridge. J Clim 12:917–932

Lau KM, Chan PH (1986) Aspects of the 40–50 day oscillation during the northern summer as inferred from outgoing longwave radiation. Mon Weather Rev 114:1354–1367

Li T, Wang B (1994) The influence of sea surface temperature on the tropical intraseasonal oscillation: a numerical study. Mon Weather Rev 122:2349–2362

Lin H (2013) Monitoring and predicting the intraseasonal variability of the east Asian–western North Pacific summer monsoon. Mon Weather Rev 141:1124–1138

Liu F, Zhou L, Ling J, Fu X, Huang G (2016a) Relationship between SST anomalies and the intensity of intraseasonal variability. Theor Appl Climatol 124:847–854

Liu F, Li T, Wang H, Deng L, Zhang Y (2016b) Modulation of boreal summer intraseasonal oscillation over the western North Pacific by the ENSO. J Clim 29:7189–7201. https://doi.org/10.1175/JCLI-D-15-0831.1

Maloney ED (2009) The moist static energy budget of a composite tropical intraseasonal oscillation in a climate model. J Clim 22:711–729

North GR, Bell TL, Cahalan RF, Moeng FJ (1982) Sampling errors in the estimation of empirical orthogonal functions. Mon Weather Rev 110:699–706

Reynolds RW, Rayner NA, Smith TM, Stokes DC, Wang W (2002) An improved in situ and satellite SST analysis for climate. J Clim 15:1609–1625

Salby ML, Hendon HH (1994) Intraseasonal behavior of clouds, temperature, and motion in the Tropics. J Atmos Sci 51:2207–2224

Teng H, Wang B (2003) Interannual variations of the boreal summer intraseasonal oscillation in the Asian–Pacifc region. J Clim 16:3572–3584

Waliser DE, Stern W, Schubert S, Lau KM (2003) Dynamic predictability of intraseasonal variability associated with the Asian summer monsoon. Q J R Meteorol Soc 129:2897–2925

Wang B, Xie X (1996) Low-frequency equatorial waves in vertically sheared zonal flow. Part I: stable waves. J Atmos Sci 53(3):449–467

Wang B, Xie X (1997) A model for the boreal summer intraseasonal oscillation. J Atmos Sci 54:72–86

Wang H, Liu H, Wang B, Li T (2018) Effect of intraseasonal oscillation on South China Sea summer monsoon onset. Clim Dyn 51(7–8):2543–2558. https://doi.org/10.1007/s00382-017-4027-9

Wu R (2010) Subseasonal variability during the South China Sea summer monsoon onset. Clim Dyn 34:629–642

Wu R (2018) Feedback of 10–20-day intraseasonal oscillations on seasonal mean SST in the tropical Western North Pacific during boreal spring through fall. Clim Dyn 51:4169–4184

Wu R, Cao X (2017) Relationship of boreal summer 10–20-day and 30–60-day intraseasonal oscillation intensity over the tropical western North Pacific to tropical Indo-Pacific SST. Clim Dyn 48:3529–3546

Wu R, Song L (2018) Spatiotemporal change of intraseasonal oscillation intensity over the tropical Indo-Pacific Ocean associated with El Niño and La Niña events. Clim Dyn 50:1221–1242

Wu R, Wang B (2001) Multi-stage onset of the summer monsoon over the western North Pacific. Clim Dyn 17:277–289

Wu R, Huang G, Du Z, Hu K (2014) Cross-season relation of the South China Sea precipitation variability between winter and summer. Clim Dyn 43(1–2):193–207

Yang J, Wang B, Wang B (2008) Anticorrelated intensity change of the quasi-biweekly and 30–50-day oscillations over the South China Sea. Geophys Res Lett 35:L16702. https://doi.org/10.1029/2008GL034449

Zhou W, Chan JCL (2005) Intraseasonal oscillations and the South China Sea summer monsoon onset. Int J Climatol 25(12):1585–1609

Zhu CW, Nakazawa T, Li JP, Chen LX (2003) The 30–60 day intraseasonal oscillation over the western North Pacific Ocean and its impacts on summer flooding in China during 1998. Geophys Res Lett 30(18):1952

**Publisher's Note** Springer Nature remains neutral with regard to jurisdictional claims in published maps and institutional affiliations.